PLANT SCIENCES

Artificial regulation of state transition for augmenting plant photosynthesis using synthetic light-harvesting polymer materials

Xin Zhou[1,2], Yue Zeng[1,2], Yongyan Tang[3], Yiming Huang[1,2], Fengting Lv[1,2], Libing Liu[1,2], Shu Wang[1,2]*

Artificial regulation of state transition between photosystem I (PSI) and PSII will be a smart and promising way to improve efficiency of natural photosynthesis. In this work, we found that a synthetic light-harvesting polymer [poly(boron-dipyrromethene-*co*-fluorene) (PBF)] with green light absorption and far-red emission could improve PSI activity of algae *Chlorella pyrenoidosa*, followed by further upgrading PSII activity to augment natural photosynthesis. For light-dependent reactions, PBF accelerated photosynthetic electron transfer, and the productions of oxygen, ATP and NADPH were increased by 120, 97, and 76%, respectively. For light-independent reactions, the RuBisCO activity was enhanced by 1.5-fold, while the expression levels of *rbcL* encoding RuBisCO and *prk* encoding phosphoribulokinase were up-regulated by 2.6 and 1.5-fold, respectively. Furthermore, PBF could be absorbed by the *Arabidopsis thaliana* to speed up cell mitosis and enhance photosynthesis. By improving the efficiency of natural photosynthesis, synthetic light-harvesting polymer materials show promising potential applications for biofuel production.

INTRODUCTION

Photosynthesis is the defining process through which green plants, algae, and cyanobacteria assimilate carbon dioxide and water to synthesize carbohydrates and release oxygen with the aid of sunlight. Owing to the fact that photosynthesis provides the materials and energy for almost all living organisms directly or indirectly, it is never an overestimation that photosynthesis builds the foundation of sustaining life on the earth (*1*). Solar irradiation delivers the most abundant renewable energy available to the earth, and its conversion to alternative forms of energy (e.g., biofuel) could potentially eliminate the problems associated with fossil fuel consumption. Among all the diverse strategies to harness solar energy, it is an effective and convenient solution to artificially improve a natural photosynthetic system.

Photosynthetic algae are not only primary producers in the ecological system but also economically valuable as a potential source of biofuel (*2*, *3*). With high metabolic activities, these microscopic synthetic factories produce a large amount of lipids, which could be extracted and converted to biofuel (*4*). However, inefficient solar-to-biofuel conversion of algae has primarily impeded the commercialization of the biofuel (*5*). The same problem was also encountered in higher plants, which use about only 1% of the total energy from absorbed sunlight (*6*). Improving photosynthetic efficiency of plants could effectively increase grain yields. The key to ameliorate the photosynthetic efficiency has been to accelerate either light-dependent reactions or light-independent reactions. To propel light-dependent reactions, efforts were mainly focused on improving light-harvesting antenna, expanding photosynthetically active radiation (PAR) spectrum and managing spectral distribution and intensity of exciting photon with light-capturing additives including phosphorescent dyes and single-walled carbon nanotubes (*7*–*12*). In the aspect of light-independent reactions, it is the principal approach to increase carbon fixation efficiency by improving ribulose-1,5-biphosphate carboxylase-oxygenase (RuBisCO) activity (*13*). However, no research has been conducted through state transition mechanism to augment photosynthesis through artificial regulation. State transition is a self-regulating mechanism in which photosynthetic apparatuses balance the excitation energy distribution between photosystem II (PSII) and PSI and improve the efficiency of light energy utilization through reversible association of light-harvesting complexes II (LHCII) between PSII and PSI (*14*). When the environmental condition favors PSII, to make the electron transport equally between PSII and PSI, LHCII is phosphorylated and migrates from PSII to PSI, thus increasing the light absorption, fluorescence intensity, and activity of PSI (state 2). Conversely, under the condition that favors PSI, LHCII is dephosphorylated and disconnects from PSI to PSII, increasing the light absorption, fluorescence intensity, and activity of PSII (state 1) (*15*). The state transition mechanism regulates the activities of photosystems and ensures efficient photosynthesis of plants. Artificial regulation of the state transition between PSI and PSII will be a smart and promising way to improve efficiency of natural photosynthesis.

The superior properties of conjugated polymers (CPs) in light-harvesting ability, fluorescence quantum yield, photostability, and biocompatibility enable their versatile applications in biological imaging, biosensing, and biomedicine (*16*–*22*). Facile structural modifications of CPs also allow the precise tailoring of their optical absorption and emission wavelengths. We have previously demonstrated that the CPs could broaden the PAR range, accelerate the electron transfer, and increase the adenosine triphosphate (ATP) formation in chloroplasts (*23*–*25*). Besides, CPs could promote progenitor cell growth via gene regulation (*26*). Here, we report an augmented photosynthesis of *Chlorella pyrenoidosa* and *Arabidopsis thaliana* with a light-harvesting CP, poly(boron-dipyrromethene-*co*-fluorene) (PBF) (Fig. 1, A and B). The cationic side chains of PBF are anticipated to bind to the negatively charged surface of *C. pyrenoidosa* through electrostatic and hydrophobic interactions. *C. pyrenoidosa* are eukaryotic algae capable of oxygenic photosynthesis. Upon PBF binding, the activity of PSI in *C. pyrenoidosa* is increased, which prompts LHCII to bind to PSII (state

[1]Beijing National Laboratory for Molecular Sciences, Key Laboratory of Organic Solids, Institute of Chemistry, Chinese Academy of Sciences, Beijing 100190, P. R. China. [2]College of Chemistry, University of Chinese Academy of Sciences, Beijing 100049, P. R. China. [3]Key Laboratory of Plant Molecular Physiology, Institute of Botany, Chinese Academy of Sciences, Beijing 100093, P. R. China.
*Corresponding author. Email: wangshu@iccas.ac.cn

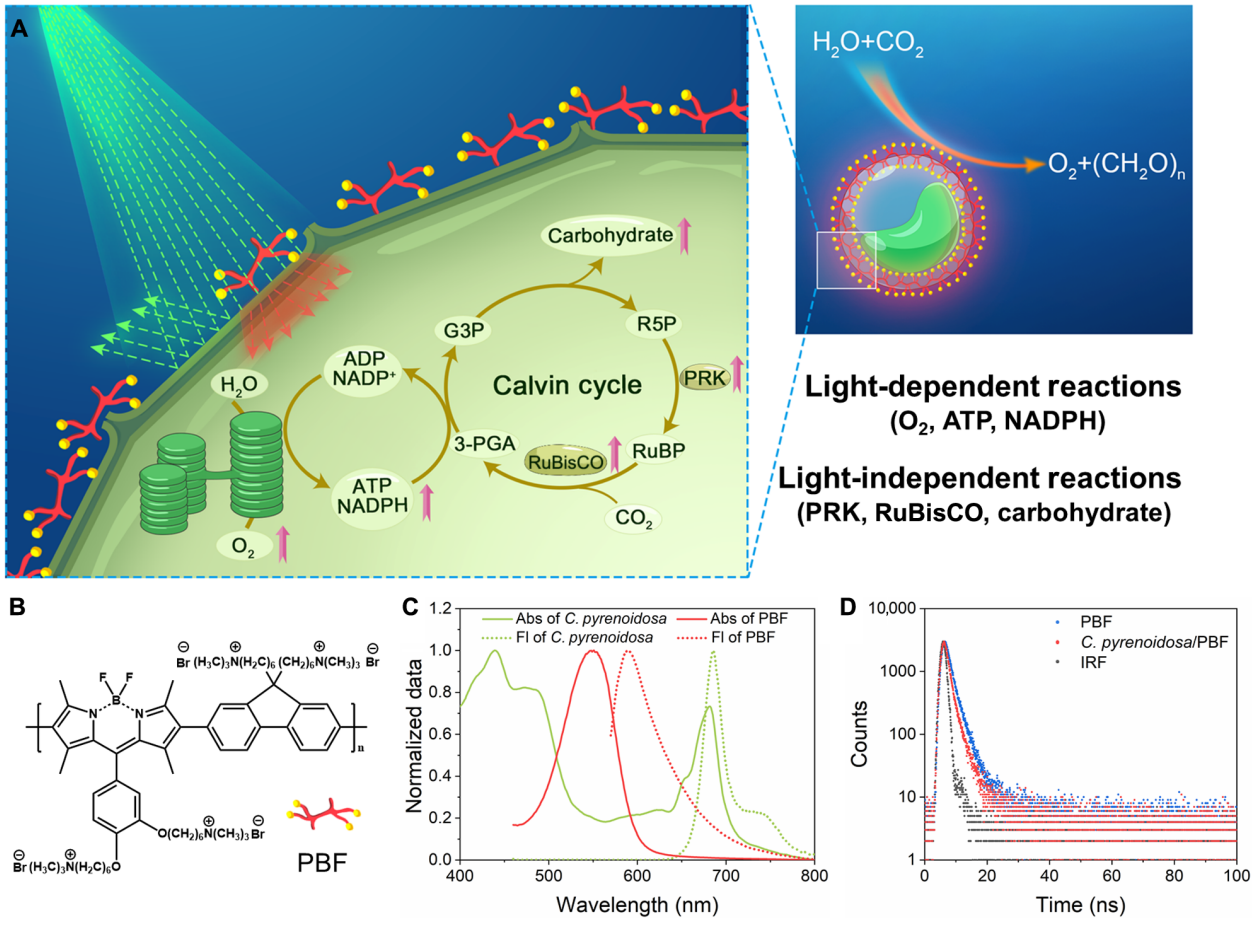

Fig. 1. Schematic diagram of CP PBF for augmenting the photosynthesis of *C. pyrenoidosa* and the spectroscopic characterization of PBF and *C. pyrenoidosa*. (**A**) PBF binds to the surface of *C. pyrenoidosa* and increases the light-dependent reaction and light-independent reactions. RuBP, ribulose 1,5-bisphosphate; 3-PGA, 3-phosphoglycerate; G3P, glyceraldehyde 3-phosphate; R5P, ribulose 5-phosphate; PRK, phosphoribulokinase. (**B**) The chemical structure of polymer PBF. (**C**) Normalized ultraviolet (UV)–visible absorption and fluorescence spectra of PBF and *C. pyrenoidosa* (λ_{ex} = 550 and 470 nm, respectively). (**D**) The fluorescence decay kinetics curves of PBF and *C. pyrenoidosa*/PBF by monitoring the emission at 610 nm with an excitation wavelength of 550 nm. IRF was the instrument response function which was measured to improve the temporal resolution of fluorescence lifetime measurements.

2 to state 1), thus increasing the activity of PSII. The overall increased activity of the photosynthetic systems results in higher photosynthetic efficiency. For light-dependent reactions, the outcome is quantified by the more rapid formation of O_2, ATP, and NADPH [reduced form of nicotinamide adenine dinucleotide phosphate ($NADP^+$)] (scheme S1). For light-independent reactions, the RuBisCO activity is noticeably enhanced and the expression levels of *rbcL* encoding RuBisCO and *prk* encoding phosphoribulokinase (PRK) are up-regulated, thus producing greater yields of lipids and proteins. Using *A. thaliana* as a model organism of higher plants, we find that the water-soluble PBF in the nutrient solution can be absorbed by roots of *A. thaliana*, allowing the plant to grow faster and bloom a week earlier than without PBF treatment.

RESULTS AND DISCUSSION

PBF polymer assembly with *C. pyrenoidosa*

The binding of PBF greatly enhanced the light utilization of *C. pyrenoidosa*. As exhibited in Fig. 1C, the absorption peaks at 440 and 470 nm of *C. pyrenoidosa* corresponded to the Soret band of chlorophylls a and b, while the peaks at 680 and 650 nm were attributed to their respective Q_y transition bands (*27*–*29*). In contrast, PBF primarily absorbed green light at 470 to 650 nm (λ_{max} = 550 nm) that was poorly captured by *C. pyrenoidosa*. Moreover, the far-red fluorescence of PBF at 570 to 800 nm (maximum at 610 nm) overlapped the absorption of *C. pyrenoidosa*, favoring the energy transfer from PBF to *C. pyrenoidosa* and thus increasing the light utilization. Furthermore, changes in the fluorescence lifetime of PBF and fluorescence spectra of *C. pyrenoidosa* before and after the formation of *C. pyrenoidosa*/PBF complex confirmed the occurrence of energy transfer (Fig. 1D and fig. S1A). The fluorescence lifetime of PBF at 610 nm decreased from 1.814 to 1.332 ns, while the fluorescence intensity of *C. pyrenoidosa* was notably increased after PBF binding to *C. pyrenoidosa* (table S1).

The cell walls of *C. pyrenoidosa* have a microfibrillar layer enclosed in a granular matrix, which are formed by polysaccharides and proteoglycans and expose a negatively charged surface (*30*, *31*). The cationic quaternary ammonium groups of PBF were anticipated to bind to *C. pyrenoidosa* surface through electrostatic interactions. The binding of PBF to *C. pyrenoidosa* surfaces was verified by confocal laser scanning microscopy (CLSM) and scanning electron microscopy (SEM). In the CLSM images (fig. S1B) and superresolution stimulated emission

depletion (STED) microscopy images (Fig. 2A), the fluorescence of PBF was mainly around the perimeter of *C. pyrenoidosa*. Three-dimensional (3D) images (Fig. 2B) confirmed the PBF fluorescence surrounding the *C. pyrenoidosa* spheroids, indicating the successful coating of PBF onto *C. pyrenoidosa* surface. SEM images revealed that *C. pyrenoidosa* alone exhibited a clean and smooth surface (Fig. 2C), while *C. pyrenoidosa*/PBF showed an uneven surface with the presence of massive aggregates (Fig. 2D). The universality of PBF enveloped *C. pyrenoidosa* was detected by flow cytometry (Fig. 2, E and F) to display the characteristics of cell population. Flow cytometry scatter plot showed that both forward scatter (FSC) and side scatter (SSC) became larger with the addition of PBF, which meant that the size and graininess of *C. pyrenoidosa* was increased. The fluorescence-activated cell sorting (FACS) analysis showed that 100% of *C. pyrenoidosa* was distributed in the single-positive region without PBF (Q2). After the addition of PBF, *C. pyrenoidosa* was 100% distributed to the double-positive area (Q3), indicating that PBF could be wrapped on the surface of all *C. pyrenoidosa*. To further investigate the interaction mechanisms, we measured isothermal titration microcalorimetry (ITC) and zeta potentials. ITC curve of titrating PBF into the *C. pyrenoidosa* suspensions was sigmoidal in shape (Fig. 2G). The initial addition of PBF yielded an exothermic observed enthalpy (ΔH_{obs}), while upon continuous

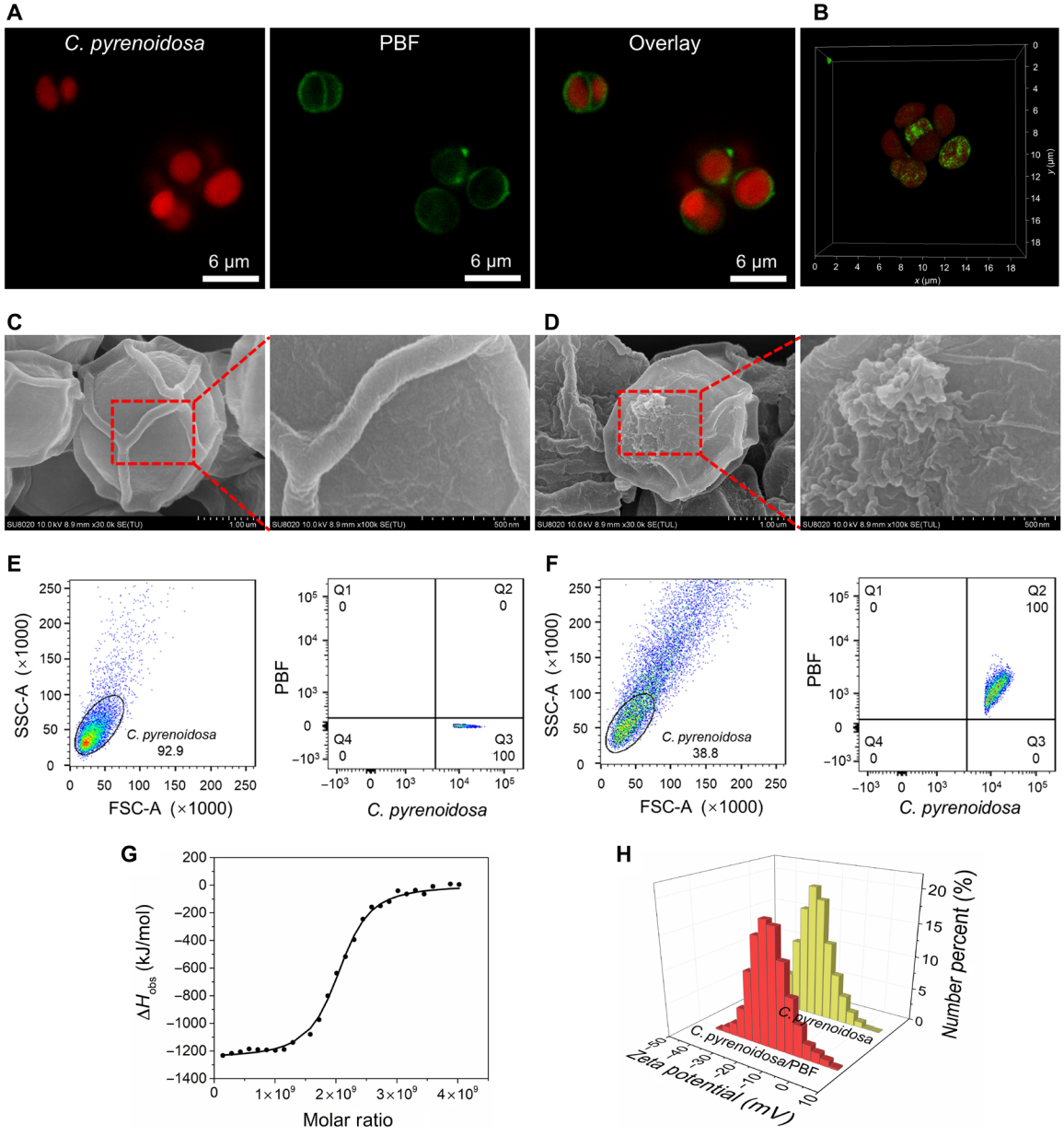

Fig. 2. Characterization of the interaction between PBF and *C. pyrenoidosa*. (**A**) Superresolution STED images and (**B**) 3D CLSM images of *C. pyrenoidosa*/PBF complexes. Red color represents *C. pyrenoidosa* (λ_{ex} = 633 nm, λ_{em} = 650 to 750 nm), and green color represents PBF (λ_{ex} = 559 nm, λ_{em} = 580 to 620 nm). SEM images of *C. pyrenoidosa* (**C**) and *C. pyrenoidosa*/PBF complexes (**D**). Flow cytometry scatter plot and FACS analysis of *C. pyrenoidosa* in the absence (**E**) and in the presence (**F**) of PBF. (**G**) Variation of observed ΔH_{obs} against the PBF/*C. pyrenoidosa* molar ratio by titrating PBF into *C. pyrenoidosa* suspensions. (**H**) Zeta potentials of *C. pyrenoidosa* before and after binding with PBF.

addition, the ΔH_{obs} became less exothermic and finally reached zero, suggesting the binding saturation of PBF on *C. pyrenoidosa* surface. The derived binding constant (K) was measured to be 2.93×10^7 M^{-1}, revealing that PBF had a high affinity toward *C. pyrenoidosa*. Besides, the exothermic ΔH_{obs} demonstrated electrostatic interaction was the dominant force for the binding (*24*). Unexpectedly, zeta potentials of *C. pyrenoidosa* only slightly shifted from −20.6 ± 0.36 to −18.5 ± 0.55 mV upon combination with PBF (Fig. 2H). Such a small difference in zeta potential implied that the PBF side chains intercalated into the cell wall of *C. pyrenoidosa* without neutralizing the negative surface charges. This intercalation was promoted by the hydrophobic interactions between PBF and the hydrophobic domain of the cell walls (*32*). Overall, both electrostatic and hydrophobic interactions made important contributions to the binding of PBF onto *C. pyrenoidosa* surface.

PBF augmentation of *C. pyrenoidosa* photosynthetic activity

C. pyrenoidosa were cultivated with different concentrations of PBF (5, 10, 20, and 50 μM) in aqueous solution. The growth vigor of *C. pyrenoidosa* was monitored by the absorbance of culture solution at 680 nm (OD_{680}) and then was correlated with the dry cell weight (DCW) via standard curve. It was noted that absorbance of PBF had negligible interference with OD_{680} (fig. S2A). As exhibited in Fig. 3A, 10 μM was the optimal PBF concentration for the accelerated growth of *C. pyrenoidosa*. Compared to the control group, the logarithmic phase of *C. pyrenoidosa* was brought ahead from day 6 to day 4. The maximum growth rate increased from 0.194 to 0.408 g d^{-1}, and the DCW increased from 0.976 to 1.118 g $liter^{-1}$. The growth of *C. pyrenoidosa* reflects the increase of overall biomass content and cell number. As photosynthetic autotrophs, their biomass is converted from photosynthetic carbon fixation. In addition, the energy and materials required for cell division are also provided by photosynthesis. Therefore, the accelerated growth of *C. pyrenoidosa* directly indicated that PBF promoted the photosynthesis of *C. pyrenoidosa*. The growth inhibition of *C. pyrenoidosa* under higher PBF concentrations (>10 μM) was attributed to excessive generation of reactive oxygen species (ROS) (fig. S2B). While 10 μM of PBF generated less ROS in comparison with 10 μM of typical cationic CP PFP [Poly (9,9-bis(6'-(*N*,*N*,*N*-trimethylammonium)hexyl)-fluorenephenylene)] and a common photosensitizer hematoporphyrin monomethyl ether (HMME), demonstrating a relatively low biotoxicity of PBF. Therefore, 10 μM PBF was selected as the optimal concentration for the following experiments.

C. pyrenoidosa as a eukaryotic alga perform oxygenic photosynthesis to produce oxygen and carbohydrates from water and carbon dioxide. Photosynthetic water oxidation is catalyzed by the oxygen evolving complex that can split water into protons, electrons, and oxygen, generating a proton gradient across the thylakoid membrane and providing electrons for photosynthetic electron transport chain. The augmented photosynthesis of *C. pyrenoidosa*/PBF was evaluated by quantification of light-dependent reaction products: O_2, ATP, and NADPH. *C. pyrenoidosa* alone produced 81.32 nmol of oxygen under light intensity of 300 μmol m^{-2} s^{-1} for 30 min, and the PBF barely produced oxygen. The *C. pyrenoidosa*/PBF hybrid increased the oxygen production by 120% (179.72 nmol) under same illumination

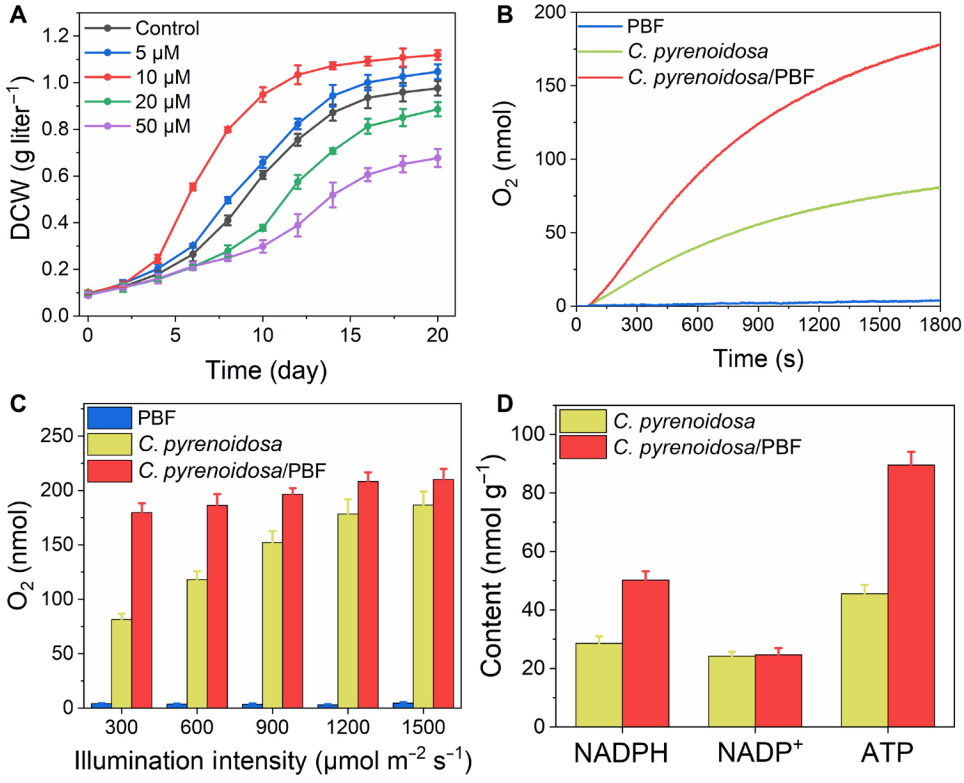

Fig. 3. The promotion of the physiological activity of *C. pyrenoidosa* by PBF. (**A**) The growth curves of *C. pyrenoidosa* cultivated in the illumination incubator in the absence or presence of PBF at different concentrations (temperature, 25°C; light intensity, 1500 lx; 12 hours of light and 12 hours of darkness). (**B**) The time course of oxygen evolution of *C. pyrenoidosa* and *C. pyrenoidosa*/PBF under illumination intensity of 300 μmol m^{-2} s^{-1}. (**C**) The quantities of oxygen evolution of *C. pyrenoidosa* and *C. pyrenoidosa*/PBF at 1800 s under different illumination intensity. (**D**) The NADPH, $NADP^+$, and ATP contents of *C. pyrenoidosa* and *C. pyrenoidosa*/PBF.

conditions, indicating a noticeably improved photosynthetic efficiency upon addition of PBF (Fig. 3B). The oxygen evolution was also measured under a series of light intensities of 300 to 1500 μmol m^{-2} s^{-1} (Fig. 3C and fig. S2). Higher light intensity increased oxygen evolution in both *C. pyrenoidosa* and *C. pyrenoidosa*/PBF. The amount of oxygen produced by *C. pyrenoidosa*/PBF was 57, 29, 16, and 12% higher than that of *C. pyrenoidosa* under the light intensity of 600, 900, 1200, and 1500 μmol m^{-2} s^{-1}, respectively. The reason for this phenomenon may be that the light gradually became saturated for *C. pyrenoidosa* as the intensity increased and the photosynthetic rate of *C. pyrenoidosa* itself gradually reached saturation as well. Therefore, PBF enabled highly efficient photosynthetic oxygen evolution of *C. pyrenoidosa* particularly under low light intensities. Furthermore, the addition of PBF increased NADPH production of *C. pyrenoidosa* from 28.57 to 50.25 nmol/g of DCW (76% increase) without affecting its $NADP^+$ content. PBF also increased ATP content of *C. pyrenoidosa* from 45.54 to 89.54 nmol/g of DCW (97% increase), thus successfully enhancing the photosynthetic efficiency of *C. pyrenoidosa* (Fig. 3D).

State transition regulation PBF synergistical improvement of PSI and PSII activity

To explain that PBF promoted *C. pyrenoidosa* light-dependent reactions, we tested the fluorescence spectra of *C. pyrenoidosa* at 77 K. The 77-K fluorescence spectrum was generally used to detect state transition, as the migration of LHCII between PSII and PSI was accompanied by their changes in fluorescence intensity. To avoid PSI reabsorbing the fluorescence of PSII, the *C. pyrenoidosa* and *C. pyrenoidosa*/PBF suspensions were adequately diluted (OD_{680} = 0.2). As displayed in Fig. 4A, the spectra of both *C. pyrenoidosa* and *C. pyrenoidosa*/PBF showed two peaks at 685 and 698 nm from the core antennae CP43 and CP47 of PSII and one peak at 718 nm from PSI (*33*). The fluorescence intensity ratio of PSI to PSII (F_{718}/F_{685} and F_{718}/F_{698}) was calculated to identify state transition (table S2). For *C. pyrenoidosa*/PBF, F_{718}/F_{685} and F_{718}/F_{698} were much lower than that of uncoated *C. pyrenoidosa*, indicating the increased electron transport (*34*). The fluorescence of PSII was distinctly enhanced, which demonstrated that *C. pyrenoidosa* cultivated with PBF were mostly in state 1 (*35*). As shown in Fig. 4B, under normal light condition, the homeostasis of *C. pyrenoidosa* tended to keep an intermediate state that LHCII transferred energy to both PSII and PSI. PBF, as a far-red emission material, could transfer the energy to *C. pyrenoidosa*, and this energy was better matched to PSI that prefers far-red light than to PSII that prefers blue light. Therefore, after *C. pyrenoidosa* were incubated with PBF, PSI became more excited *(36)*. The activity of PSII was unable to offer enough electrons for PSI. The transfer rate of electrons from PSII flowed out of plastoquinone (PQ) pool in the electron transport chain was faster than that of electrons flowed into PQ. As a result, PQ was oxidized to inactivate LHCII kinase but activate phosphatase. Thus, the phosphorylated LHCII was dephosphorylated by phosphatase and disconnected from PSI to join PSII. The state transition phenomenon indicated that PBF enhanced the activity of PSI and then further improved the activity of PSII.

Light-dependent reactions are critically dependent on PSII-related water hydrolysis and accompanying linear photosynthetic electron transfer. To further investigate the differences in behaviors of photosynthetic activity of PSII between *C. pyrenoidosa* and *C. pyrenoidosa*/PBF, the absorption and capture of light energy and the process of photosynthetic electron transfer were examined by measuring the chlorophyll fluorescence transient curve of *C. pyrenoidosa* under dark adaptation using Handy PEA continuous excitation fluorimeter (*37*). The chlorophyll fluorescence kinetics curves were exhibited in Fig. 4C, and their obtained chlorophyll fluorescence parameters and physiological significance were shown in Fig. 4D and table S3 (*38*). Apparently, ABS/RC, TR_o/RC, ET_o/RC, RE_o/RC, ABS/CS_m, TR_o/CS_m, ET_o/CS_m, and RE_o/CS_m were all notably improved, which indicated that all the efficiency of energy absorption, capture, and transfer in electron transport chain were enhanced for *C. pyrenoidosa* cultured with PBF (Fig. 4E). Thus, PI_{abs} and PI_{total} were boosted obviously, which were essential indicators for *C. pyrenoidosa* vitality. After cultured with PBF, the S_m of *C. pyrenoidosa* increased, indicating that the size of PQ pool was enlarged and more electrons flowed from PQ to the electron transport chain, which was consistent with the results of 77-K fluorescence measurements. Notably, the minor change of F_v/F_m was due to the synchronous increase of absorbed and trapped energy. Furthermore, the modulated chlorophyll fluorescence of *C. pyrenoidosa* under light adaptation were measured with FMS-2 pulse-modulated fluorimeter to determine the relative extent of photochemical and nonphotochemical process following the absorption of light energy by antenna molecules. As shown in Fig. 4F, the actual photochemical efficiency of *C. pyrenoidosa* (ϕPSII) increased by 16% under test condition after cultivation of *C. pyrenoidosa* with PBF, indicating that more proportional light energy absorbed by PSII was converted to photochemical energy. Simultaneously, the photochemical quenching coefficient (qP) that represented the proportion of absorbed energy transferred to photochemical apparatus was increased by 5%, and non-qP (qNP) such as heat loss was decreased by 21%. Besides, the electron transfer rate (ETR) was accelerated by 16%. Moreover, parallel tests were performed on PBF alone to eliminate the possible interferences from the fluorescence of PBF, and the results showed the negligible relativity of PBF to that of *C. pyrenoidosa* under test condition (Fig. 4C and table S4). In conclusion, PBF increased the operating efficiency of photosynthetic apparatus in PSII including light absorption, capture, utilization, and electron transfer.

PSI operates in series with PSII in photosynthetic electron transport chain. PSI reenergizes the electrons from PSII and transfers them to ferredoxin for the NADPH production. The activity of PSI depends on light-harvesting capacity and trapping efficiency, which varies under different environmental conditions (*39*). The 77-K fluorescence spectra have proven that PBF could increase the PSI activity of *C. pyrenoidosa*. To further confirm this claim, we evaluated the PSI electron transport and the redox kinetics of P700 (a chlorophyll species in PSI and the primary electron donor of PSI). As shown in Fig. 4G, the effective photochemical quantum yield of PSI, *Y*(I), in *C. pyrenoidosa*/PBF was 0.71 ± 0.02, which was distinctly larger than that in *C. pyrenoidosa* (0.63 ± 0.04). The increase of *Y*(I) made it clear that PBF could improve the PSI activity and accelerated PSI electron transport. The nonphotochemical PSI quantum yield of acceptor-side limited heat dissipation, *Y*(NA), decreased from 0.13 ± 0.05 to 0.05 ± 0.02 after cultivation of *C. pyrenoidosa* with PBF, implying that P700 could be oxidized more efficiently. The nonphotochemical PSI quantum yield of donor-side limited heat dissipation, *Y*(ND), barely changed, suggesting that the P700 reduction was not affected. We evaluated the P700 redox kinetics through measuring the absorption changes at 705 nm (ΔAbs_{705}) of *C. pyrenoidosa* during the process of P700 oxidation and reduction. P700 was oxidized, induced by a continuous illumination with a 720-nm actinic light-emitting diode (LED), followed by its reduction in the dark. As shown in Fig. 4H, *C. pyrenoidosa*/PBF had a larger maximum ΔAbs_{705}

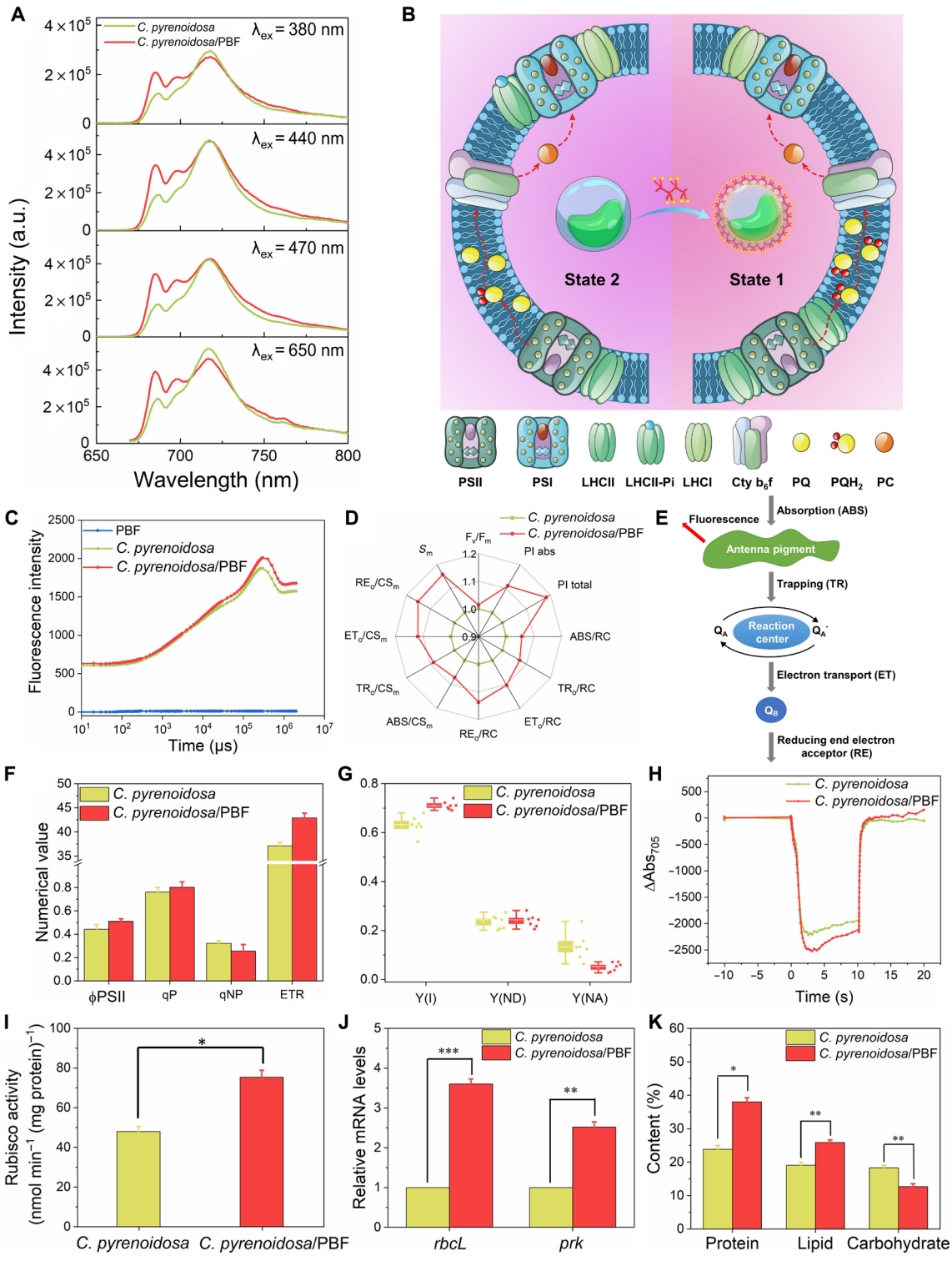

Fig. 4. The improvement of PBF on the light-dependent reactions and light-independent reactions of *C. pyrenoidosa*. (**A**) The fluorescence emission spectra of *C. pyrenoidosa* and *C. pyrenoidosa*/PBF (λ_{ex} = 380, 440, 470, and 650 nm) at 77 K. (**B**) Schematic diagram of PBF induced state transition of *C. pyrenoidosa*. PBF improved PSI activity, which made more LHCII be combined to PSII and more *C. pyrenoidosa* in state 1. (**C**) Chlorophyll fluorescence kinetics curves of PBF, *C. pyrenoidosa*, and *C. pyrenoidosa*/PBF. (**D**) The spider plot of chlorophyll fluorescence parameters of *C. pyrenoidosa* and *C. pyrenoidosa*/PBF under dark adaptation. (**E**) A simplified scheme for energy cascade from light absorption to electron transport. (**F**) Chlorophyll fluorescence characteristics of *C. pyrenoidosa* and *C. pyrenoidosa*/PBF under light adaptation. (**G**) PSI quantum yields in *C. pyrenoidosa* and *C. pyrenoidosa*/PBF. (**H**) P700 kinetics tested by monitoring changes in absorbance at 705 nm during a 20-s illumination. (**I**) The RuBisCO activity of *C. pyrenoidosa* cultured in the presence and absence of PBF. (**J**) Relative mRNA expression level of *rbcL* and *prk* in *C. pyrenoidosa* cultured in PBF. (**K**) The protein, lipid, and carbohydrate contents in *C. pyrenoidosa* cultured in the presence and absence of PBF. *P < 0.05, **P < 0.01, and ***P < 0.001 relative to control (Tukey's test). a.u., arbitrary units.

than *C. pyrenoidosa*. The results demonstrated that more P700 was oxidized at the same time, which was consistent with the results of *Y*(I) measurements and proved a higher PSI activity.

PBF acceleration of light-independent reactions for *C. pyrenoidosa*

Augmented photosynthesis also requires equivalently highly efficient light-independent reactions to coordinate with the light-dependent reactions. Therefore, we measured the activity and expression level of the RuBisCO in *C. pyrenoidosa*. RuBisCO is the crucial enzyme that is responsible for carbon dioxide fixation. It catalyzes the addition of carbon dioxide to ribulose-1,5-biphosphate, which is the rate-limiting step in Calvin cycle (*13*, *40*). The addition of PBF uplifted the RuBisCO activity from 48.04 to 75.38 nmol (min·mg·protein)$^{-1}$ (Fig. 4I) corresponding to a 57% rise. Then, we examined the expression levels of *rbcL* and *prk* using quantitative real-time polymerase chain reaction (Fig. 4J). PRK is another essential enzyme in Calvin cycle that catalyzes the phosphorylation of ribulose-5-phosphate and regenerates ribulose-1,5-bisphosphate. It is gratifying that the expression levels of *rbcL* and *prk* were notably up-regulated to 3.6- and 2.5-fold of the control, respectively. PBF could prominently enhance the activity of RuBisCO and expression levels of *rbcL* and *prk*, which exhibited

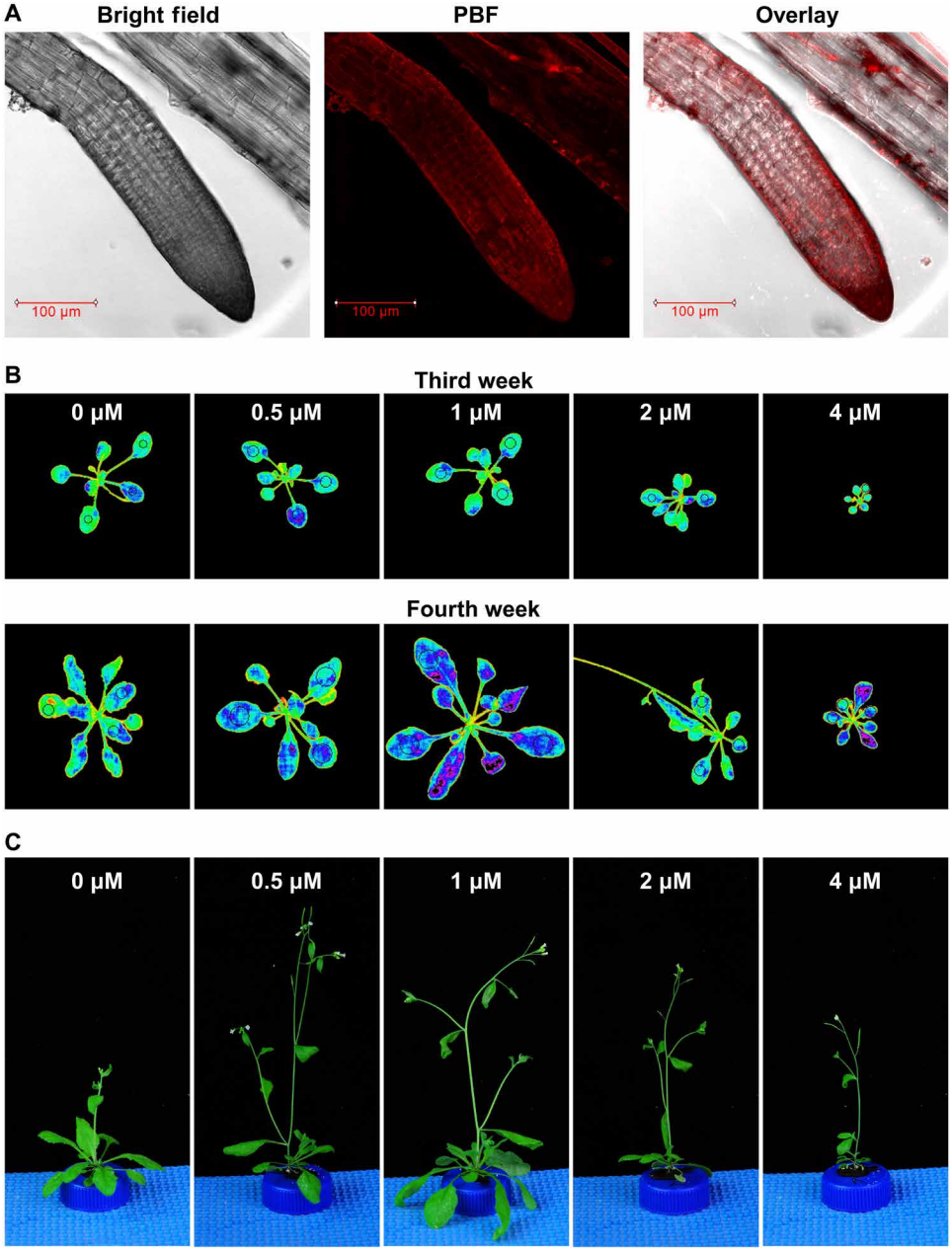

Fig. 5. The effect of PBF on growth phenotype of *A. thaliana*. (**A**) CLSM images of the roots of *A. thaliana* that were grown in growth medium containing PBF. Red color represents PBF (λ_{ex} = 559 nm; λ_{em} = 580 to 620 nm). (**B**) Chlorophyll fluorescence imaging of *A. thaliana* that were grown in growth medium containing different concentration of PBF at the third and fourth week. (**C**) The photographs of *A. thaliana* that were grown in growth medium containing different concentration of PBF at the fifth week. Photo credit: X. Zhou, Chinese Academy of Sciences.

that PBF could accelerate the light-independent reaction rate of photosynthesis as well.

Photosynthesis is responsible for supplying almost all the organic compounds required to sustain life on the earth. Increasing the yield of organic compounds in photosynthesis is meaningful for the biosystem and anticipated to mitigate climate change and energy scarcity. As shown in Fig. 4K, the protein, lipid, and carbohydrate contents were 24, 19, and 18% DCW, respectively. After *C. pyrenoidosa* was cultivated with PBF, the protein and lipid contents were increased to 38 and 26%, while carbohydrate content was decreased to 13%. This was attributed to carbohydrate synthesized by light-independent reactions was converted into protein and lipid. Cultivation with PBF raised overall biomass content of *C. pyrenoidosa* from 61 to 77% DCW.

PBF augmentation of *A. thaliana* photosynthetic activity

We further explored the utilization of PBF in augmenting photosynthesis of a higher plant model *A. thaliana*. The PBF was highly soluble in the growth medium for *A. thaliana* and was readily absorbed by the roots of *A. thaliana*. CLSM images of the root sample showed that PBF was in root crown, meristematic zone to elongation zone (Fig. 5A). Chlorophyll fluorescence imaging was used to monitor the effect of PBF on the growth and photosynthesis of *A. thaliana*. In the third week after sowing, the effect of low-concentration PBF (0.5 and 1 μM) on the growth phenotype of *A. thaliana* was not obvious. However, high-concentration PBF (4 μM) visibly inhibited growth (Fig. 5B). By the fourth week, the effect of low-concentration PBF was evident, which promoted the growth of *A. thaliana*, and 1 μM was the optimal concentration. Besides, bolting

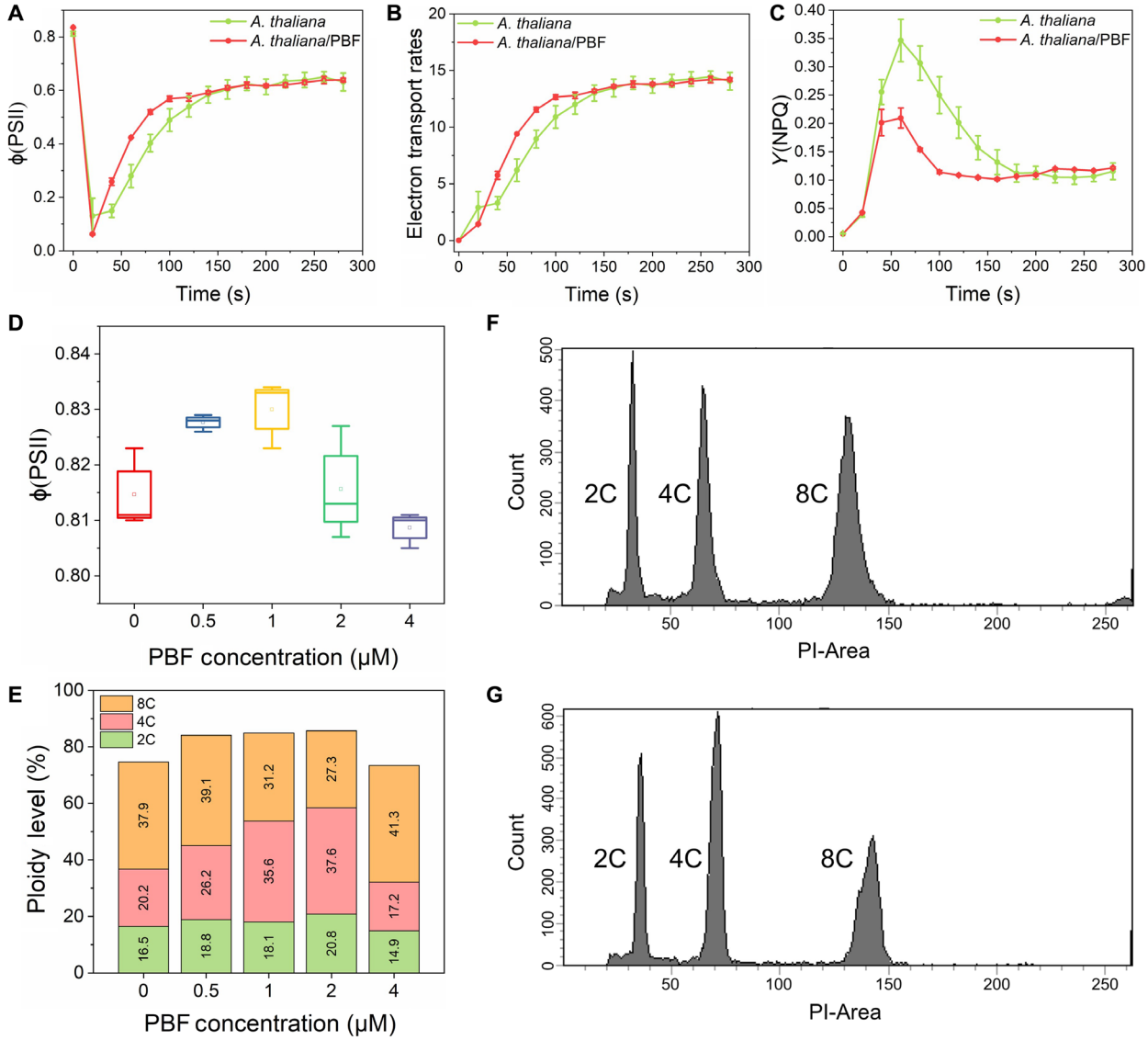

Fig. 6. The effect of PBF on photosynthesis and cell cycle of *A. thaliana*. Chlorophyll fluorescence kinetics of *A. thaliana* at the third week, including effective PSII quantum yield *Y*(II) (**A**), electron transport rate (**B**), and quantum yield of light induced nonphotochemical quenching *Y*(NPQ) (**C**). The concentration of PBF was 1 μM. (**D**) The photochemical efficiency (ϕPSII) of *A. thaliana* at the third week that were grown in growth medium containing different concentration of PBF. (**E**) The nuclear ploidy distributions of *A. thaliana* at the third week that were grown in growth medium containing different concentration of PBF. Flow cytometry histograms for the ploidy analysis of *A. thaliana* (**F**) and *A. thaliana* treated with 1 μM PBF (**G**).

was observed in *A. thaliana* treated with PBF. Starting from the fifth week, we tracked the *A. thaliana* growth by photographs because the plant was too tall for chlorophyll fluorescence imaging. As exhibited in Fig. 5C, PBF-treated *A. thaliana* started flowering, while the control group just began to bolt. In addition, 1 μM PBF-treated *A. thaliana* was stronger and taller. Therefore, phenotypic studies have shown that low concentrations of PBF could promote the growth of *A. thaliana* and advance its flowering time by 1 week. Besides, there had no traces to show the toxicity of PBF to plants in the concentration range that we studied. Although high-concentration PBF inhibited the growth of *A. thaliana*, the plants still carried out photosynthesis, growing to bolting, flowering, and fruiting. When the PBF concentration reached to 10 μM, still no obviously phenomenon of cell or plant death was found (fig. S3). Thus, we speculated that high concentration of PBF caused a stress condition rather than toxicity to plants.

To investigate the effect of PBF on photosynthesis of *A. thaliana*, chlorophyll fluorescence data were monitored. After dark adaptation, *A. thaliana* treated with PBF recovered to the plateau stage earlier, indicating that PBF accelerated the initiation of photosynthesis (Fig. 6, A to C, and fig. S4). At the third week, PBF reduced the nonphotochemical quenching efficiency of *A. thaliana*, allowing more absorbed energy to be used for photosynthesis. What is more, 1 μM PBF substantially improved the photochemical efficiency of *A. thaliana*. While at higher concentration, PBF inhibited the photochemical efficiency, which was consistent with phenotypic studies (Fig. 6D). The growth promotion of PBF on *A. thaliana* was further studied with flow cytometry (Fig. 6, E to G, and fig. S5). At the third week, 2C, 4C, and 8C cells in the control group accounted for 17, 20, and 38%, respectively. After adding PBF with growth-promoting concentration, the ratio of 2C cells changed little, while that of 4C cells increased substantially. The increased ratio of 4C/2C indicated that PBF accelerated the progression of G_1-S phase to G_2-M phase and accelerated the rate of mitosis, and for 4 μM PBF, it retards the process of mitotic cell cycle and stunts plant growth (*41*). The results of the fourth week were consistent with that of the third week. Therefore, low concentration of PBF can augment photosynthesis and mitosis of *A. thaliana* and promote its growth.

CONCLUSION

In summary, light-harvesting polymer PBF has been modified on the surface of algae *C. pyrenoidosa* via electrostatic and hydrophobic interactions, achieving the acceleration of light-dependent and light-independent reactions simultaneously and ultimately augmenting its photosynthesis. PBF brought forward the logarithmic growth stage of *C. pyrenoidosa* with maximum growth rate increased by 110%. PBF could induce synergistical improvement of PSI and PSII activity through regulating their state transition. As a result, the oxygen evolution and the ATP and NADPH contents were notably increased. Cultivated with PBF, the RuBisCO activity of *C. pyrenoidosa* was enhanced by 57% and the expression levels of *rbcL* and *prk* were up-regulated to 3.6- and 2.5-fold, leading to obvious increase of lipid and protein production. Furthermore, PBF can be absorbed by the roots of *A. thaliana* to improve its photosynthesis and accelerate cell mitosis, resulting in faster growth and earlier flowering. With excellent harvesting ability to green light, water solubility, and biocompatibility, synthetic polymer materials show promising potential applications for biofuel production, as well as for future energy and environmental development.

MATERIALS AND METHODS

Materials and instruments

All the chemicals used in experiments were purchased from Innochem, Alfa Aesar, J&K, or Sigma-Aldrich. PBF was prepared according to the procedures in the literature (*42*).The green microalgae *C. pyrenoidosa* were purchased from Freshwater Algae Culture Collection at the Institute of Hydrobiology. *C. pyrenoidosa* were cultured in BIC-250 illumination incubator (Shanghai Boxun Industrial Co. Ltd., China). ATP assay kit (colorimetric/fluorometric) was purchased from Abcam. BCA protein quantification kit was purchased from Abcam. Amplite fluorimetric NADP/NADPH ratio assay kit was purchased from AAT Bioquest Inc. Spurr resin was purchased from Ted Pella Inc. Ultraviolet (UV)–visible absorption spectra were recorded on evolution 201 UV-visible spectrophotometers (Thermo Fisher Scientific, USA). Fluorescence spectra were taken on Hitachi F-4600 fluorimeter equipped with a xenon lamp excitation source. The 77-K fluorescence spectra and decay kinetics were measured using FLS980 spectrometer (Edinburgh Instruments, UK). The oxygen evolution was measured with chlorolab-2 liquid-phase oxygen electrode systems (Hansatech, UK). The photosynthetic activities of PSII were tested with Handy PEA chlorophyll fluorimeter and FMS-2 pulse-modulated fluorimeter (Hansatech, UK), and the photosynthetic activities of PSI were measured with Dual-PAM-100 (Walz, Germany) and JTS-10 pump-probe spectrometer (BioLogic, France). Isotherm titration microcalorimetry was taken on TAM III microcalorimetric system with a stainless-steel sample cell of 1 ml. Transmission electron microscope images were viewed with JEOL JEM1230. SEM images were viewed with Hitachi SU8020 SEM. Zeta potentials were taken on Malvern Zetasizer Nano ZS90 (ZEN3600). CLSM images and STED ultrahigh-resolution microscopy images were viewed with confocal laser scanning biological microscope (Leica SP8 STED 3X, Germany). Chlorophyll fluorescence imaging was taken with Imaging-PAM (Waltz, Germany). Nuclei extraction and DNA staining were done with CyStain PI Absolute P. Flow cytometry was measured with BD LSRFortessa cell analyzer.

Methods

C. pyrenoidosa culture

C. pyrenoidosa were cultured with BG-11 medium in the illumination incubator (temperature, 25°C; light intensity, 1500 l×; 12 hours of light and 12 hours of darkness). The culture flasks were artificially shook three times per day. The concertation of *C. pyrenoidosa* was determined by the absorbance at 680 nm (OD_{680}). The components of BG-11 medium were as follows: $NaNO_3$ (1.5 g/liter), Na_2CO_3 (0.02 g/liter), K_2HPO_4 (0.04 g/liter), $MgSO_4$ $7H_2O$ (0.075 g/liter), $CaCl_2$ $2H_2O$ (0.036 g/liter), citric acid (6 mg/liter), ferric ammonium citrate (6 mg/liter), EDTA Na_2 (1 mg/liter), and trace metal solution (1 ml/liter). The trace metal solution consisted of H_3BO_3 (2.86 g/liter), $MnCl_2$ $4H_2O$ (1.86 g/liter), $ZnSO_4$ $7H_2O$ (0.22 g/liter), Na_2MoO_4 $2H_2O$ (0.39 g/liter), $CuSO_4$ $5H_2O$ (0.08 g/liter), and $Co(NO_3)_2$ $6H_2O$ (0.05 g/liter).

CLSM and STED ultrahigh-resolution microscopy

C. pyrenoidosa and *C. pyrenoidosa*/PBF were collected by centrifuging at 7000 rpm for 5 min and washed with phosphate-buffered saline (pH 7.4) three times. Then, 5-μl suspensions were dropped on a glass slide and covered with a coverslip. The samples were viewed and imaged with CLSM. The excited lasers were 488 and 559 nm for *C. pyrenoidosa* and PBF, respectively. For STED ultrahigh-resolution microscopy, the excited laser of *C. pyrenoidosa* was 633 nm and the collected fluorescence band was 660 to 750 nm. The STED laser was 775 nm.

The excited laser of PBF was 559 nm, and the collected fluorescence band was 580 to 620 nm. The STED laser was 660 nm.

Isotherm titration microcalorimetry

C. pyrenoidosa suspensions (600 μl; OD_{680} = 1) or BG-11 medium (600 μl) were added into the sample cell, and then, PBF solution (100 μM) was consecutively injected into the stirred sample cell (stirring rate was 60 rpm) in amounts of 10 μl via a 500-μl Hamilton syringe controlled by a Thermometric 612 Lund pump until the interaction progress was completed. The isotherm titration microcalorimetry was repeated three times with the deviation within ±4%. The dilution enthalpies of PBF were subtracted from the corresponding observed enthalpy of PBF titrating *C. pyrenoidosa* suspensions.

SEM and transmission electron microscopy measurements

C. pyrenoidosa and *C. pyrenoidosa*/PBF were collected by centrifuging at 7000 rpm for 5 min. The precipitate was rinsed three times with deionized water, and the supernatant was discarded. The cells were first fixed in 2.5% (w/v) glutaraldehyde for 6 hours at 4°C, followed by the rinsing of 0.1 M phosphate-buffered saline (pH 7.4) three times. Then, the cells were further fixed with 0.5% (w/v) osmic acid for 3 hours and washed with 0.1 M phosphate-buffered saline (pH 7.4) three times. After that, the cells were dehydrated by rinsing in a graded series of ethanol (50, 70, 80, 90, 95, and 100%, for 15 min). For SEM, cells were dropped onto silicon slice followed by drying in the air. The specimens were sputtered with platinum and viewed with a scanning electron microscope. For transmission electron microscopy, cells were embedded in Spurr resin and polymerized for 48 hours at 70°C. Ultrathin sections (60 to 80 nm thick) were prepared and stained with 2% (w/v) uranium acetate and lead citrate. After drying at room temperature, the samples were viewed with a transmission electron microscope.

Zeta potential measurements

C. pyrenoidosa were incubated with 10 μM PBF for 30 min in the illumination incubator. The *C. pyrenoidosa* suspensions were centrifuged to remove the unbound PBF (7000 rpm, 5 min). The pellets were washed with Milli-Q water and resuspended in Milli-Q water for zeta potential measurements. Then, the untreated *C. pyrenoidosa* were measured in the same conditions.

The growth curve of C. pyrenoidosa

C. pyrenoidosa at logarithmic phase were inoculated into 100 ml of fresh BG-11 medium. For *C. pyrenoidosa*/PBF, 1 mM PBF was added to the medium with a final concentration of 10 μM. *C. pyrenoidosa* and *C. pyrenoidosa*/PBF were cultured in the illumination incubator (temperature, 25°C; light intensity, 1500 l×; 12 hours of light and 12 hours of darkness). The culture flasks were artificially shook three times per day. OD_{680} were recorded every 2 days. Then, OD_{680} was correlated with the DCW via standard curve. The standard curve equation was

$$\mathrm{DCW\ (g\ liter^{-1})} = 0.2105 \times \mathrm{OD_{680}} + 0.00624, R^2 = 0.993$$

The growth rate was calculated using the equation

$$\mu = \frac{\ln(N_1) - \ln(N_0)}{t_1 - t_0}$$

where t_1 and t_0 were cultivation time and N_1 and N_0 were the DCW at t_1 and t_0, respectively. The experiment was carried out in parallel with three groups, and the growth curve was derived from the average value.

ROS generation

DCFH-DA (2, 7-dichlorofluorescein diacetate) was dissolved in ethanol and activated in 0.01 M NaOH to get DCFH. DCFH (200 μl; 40 μM) was added into wells of 96-well plates, and then, 10 μl of different concentrations of PBF (the final concentrations were 0, 5, 10, 20, and 50 μM), poly(*p*-phenylenevinylene), and HMME were placed in each well. The samples were irradiated in illumination incubator under the same condition as that of *C. pyrenoidosa* culturing. The fluorescence intensity of DCF which was the oxidation product of DCFH at 525 (excitation 488 nm) was recorded every 1 min.

Oxygen evolving activity measurements

The photosynthetic oxygen evolving activities of *C. pyrenoidosa* and *C. pyrenoidosa*/PBF were estimated with Clark-type oxygen electrode. Cell suspensions (2 ml) in the logarithmic phase were collected by centrifugation and resuspended in the fresh BG-11 medium at the concentration of OD_{680} = 2. Then, 2-ml cell resuspensions were loaded in the oxygen electrode chamber. Twenty microliters of 0.1 mM sodium bicarbonate was added to the chamber, which provided adequate carbon source to the *C. pyrenoidosa*. The solution was purged with nitrogen for 15 min to deoxygenate. The oxygen evolving amount was monitored under different illumination intensity (300, 600, 900, 1200, and 1500 μmol m^{-2} s^{-1}) at 25°C.

Seventy-seven–kelvin fluorescence spectroscopy and fluorescence decay kinetics curves

The *C. pyrenoidosa* and *C. pyrenoidosa*/PBF were adjusted to the concentration of OD_{680} = 1 and added to fluorimeter cuvettes (path length was 10 mm). The samples were cooled to 77 K in liquid nitrogen. The fluorescence spectra were recorded under excitation wavelength of 380, 440, 470, 550, and 650 nm. The slit width of monochromator was 2 nm for exciting light and 5 nm for emitted light. The fluorescence decay kinetics curves were measured by monitoring the emission at 680 nm under excitation wavelength of 440 nm. The spectra were fitted with a three–exponential decay function with a global analysis method.

Chlorophyll fluorescence kinetics measurements

Photosynthetic activities of *C. pyrenoidosa* and *C. pyrenoidosa*/PBF were evaluated by fast chlorophyll fluorescence kinetics curves using Handy PEA chlorophyll fluorimeter and FMS-2 pulse-modulated fluorimeter. First, 2-ml *C. pyrenoidosa* or *C. pyrenoidosa*/PBF suspensions were added to sample bottles and kept in the dark for 30 min to make the PSII reaction center completely open and electron transport chain fully oxidized. Then, the bottles were placed in Handy PEA or FMS-2 liquid phase detector and measured.

Photosynthetic activities of PSI measurements

C. pyrenoidosa or *C. pyrenoidosa*/PBF suspensions (2 ml) were added to sample bottles and kept in the dark for 15 min. The measure mode was P700, and the analysis method was saturation pulse analysis. The actinic light source was red light, and the measurement light intensity was 50 μmol m^{-2} s^{-1}. For JTS-10 measurements, the LED far-red light intensity was 1400 μmol m^{-2} s^{-1}. The optical change of the *C. pyrenoidosa* at 705 nm was monitored during 20 s of illumination.

RuBisCO activity measurements

C. pyrenoidosa and *C. pyrenoidosa*/PBF were collected by centrifuging at 7000 rpm for 5 min. The precipitate was resuspended in 1 ml of extraction buffer [10 mM $MgCl_2$, 0.25 mM EDTA, and 40 mM tris-HCl buffer (pH 7.6)] and subsequently ground in ice bath with quartz sand. The homogenate was centrifuged at 20,000*g* for 15 min at 4°C to get the supernatant. Total RuBisCO activity was measured by placing 50 μl of supernatant in 1 ml of assay buffer [40 mM tris-HCl buffer (pH 7.8), 0.4 mM EDTA-Na_2, 12 mM $MgCl_2$,

10 mM ATP, 1 mM reduced form of NAD^+, 40 mM $NaHCO_3$, 10 mM creatine phosphate, 20 U of creatine phosphate kinase, 20 U of phosphoglyceric kinase, and 20 U of phosphoglyceraldehyde dehydrogenase]. The reaction was initiated with 5 mM ribulose-1,5-biphosphate, and the absorbance at 340 nm was monitored every 10 s in 1 min. The activity was determined by the rate of decrease in absorbance.

Quantitative reverse transcription polymerase chain reaction

The total RNA of *C. pyrenoidosa* was extracted using the TRIzol reagent. The integrity of the total RNA was identified using agarose gel electrophoresis. The cDNA was obtained by reverse transcription using TIANScript RT Reagent Kit, where 1 μg of total RNA was used as a template. The specific primers of two genes, which were related to two critical enzymes (RuBisCO and PRK) in light-independent reactions of photosynthesis, were designed (Table 1). The housekeeping gene β-actin served as internal control. The expression level of the target genes was calculated according to the $2\Delta\Delta CT$ method and normalized against that of internal control.

Measurement of carbohydrate content

C. pyrenoidosa and *C. pyrenoidosa*/PBF were collected by centrifuging at 7000 rpm for 5 min. The precipitate was put into an oven to dry (85°C, 12 hours). Dried cells (100 mg) were immersed in 10 ml of 80% ethanol and stirred for 30 min in 80°C water bath. Then, the mixture was centrifuged at 12,000 rpm for 10 min to obtain supernatant. The residue was repeatedly extracted with 80% ethanol, and supernatant was combined. The 1-ml extraction was added into the 5-ml anthrone test solution [anthrone (1 g/ml)/80% H_2SO_4]. The mixture was boiled in a boiling bath for 10 min, and the absorbance at 625 nm (OD_{625}) was detected. The carbohydrate content was calculated via carbohydrate content–OD_{625} standard curve. The standard curve was protracted by treating a series of glucose solutions with the same method and measuring OD_{625}.

Measurement of protein content

C. pyrenoidosa (10 ml) and *C. pyrenoidosa*/PBF (10 ml) at the same OD_{680} were collected by centrifuging at 7000 rpm for 5 min. The precipitate was resuspended in 10 ml of phosphate-buffered saline buffer and subsequently ground in ice bath with quartz sand. The homogenate was centrifuged at 13,000*g* for 5 min at 4°C to get the supernatant. The protein content was measured with BCA Protein Assay Kit.

Measurement of lipid content

C. pyrenoidosa and *C. pyrenoidosa*/PBF were collected by centrifuging at 7000 rpm for 5 min. The precipitate was put into an oven to dry (85°C, 12 hours). The dried cells were cooled in a dryer and weighed (M_1). The cells were immersed in diethyl ether for 16 hours and then extracted in a Soxhlet extractor for 6 hours. The sample was dried and weighed (M_2). The lipid content was calculated as

$$\text{Lipid Content} = \frac{M_1 - M_2}{M_1} \times 100\%$$

Table 1. Primers for quantitative reverse transcription polymerase chain reaction detection of expression genes in *C. pyrenoidosa*.

Gene	Primer sequence (5′→3′)	Length of production
prk	AGGAGAAGGCGGTGACTG	116
	GACGTGGTTGTAGATGGG	
rbcL	AAACTGGTGAAATTAAAGGGC	195
	CACGGTGAATGTGTAAAAGAA	
β-Actin	TTTGACTCAACACGGGAAAAC	115
	CAACCCACCAACTAAGAACGG	

Measurement of ATP content

C. pyrenoidosa and *C. pyrenoidosa*/PBF were collected by centrifuging at 7000 rpm for 5 min. The precipitate was resuspended in 1 ml of ATP assay buffer and subsequently ground in ice bath with quartz sand. The homogenate was centrifuged at 13,000*g* for 5 min at 4°C to get the supernatant. The ATP content was measured with ATP assay kit (colorimetric/fluorometric).

Measurement of NADP/NADPH content

C. pyrenoidosa and *C. pyrenoidosa*/PBF were collected by centrifuging at 7000 rpm for 5 min. The precipitate was resuspended in 1 ml of cells lysis buffer and subsequently ultrasonicated for 30 min in ice bath. The solution was centrifuged at 7000 rpm for 5 min at 4°C to get the supernatant. The NADP/NADPH content was measured with an Amplite fluorimetric NADP/NADPH ratio assay kit.

Hydroponic growth of A. thaliana

A. thaliana (ecotype Columbia) seeds were placed in distilled water and left in the dark at 4°C for 3 days for vernalization. The lid of the 1.5-ml black centrifugal tube was cut off, and a 2-mm hole was punched with a puncher. The lid was filled with the germination medium, which was used as the seed holder. Then, the seed holder was placed on the perforated foam plate and floated on growth medium. The vernalized seeds were seeded into the hole in the lid. The seeds were placed in plant culture room (temperature, 23°C; light intensity, 5000 l×; 16 hours of light and 8 hours of darkness) for 10 days. During this time, the seeds would germinate and grow cotyledons and, then, true leaves. The conical bottom of a 50-ml centrifuge tube was cut off, and a hole that could support the seed holder was punched in the lid, and the 50-ml centrifuge tube was placed in a foam plate with suitable holes and floated on growth medium. The seed holder was transplanted into the modified 50-ml centrifuge tube. PBF was added to the growth medium (the concentration was 0.5, 1, 2, and 4 μM). The seedlings were raised in a plant culture room [KH_2PO_4 (34 mg/liter), $MgSO_4$ (60 mg/liter), KNO_3 (202 mg/liter), NH_4NO_3 (40 mg/liter), $Ca(NO_3)_2$ (472 mg/liter), H_3BO_3 (1.546 mg/liter), $MnCl_2$ (0.396 mg/liter), $ZnSO_4$ (0.575 mg/liter), $CuSO_4$ (0.125 mg/liter), KCl (3.725 mg/liter), $CoCl_2$ (0.035 mg/liter), $(NH_4)_2MoO_4$ (0.093 mg/liter), and FeNaEDTA (16.8 mg/liter)].

Chlorophyll fluorescence imaging

Chlorophyll fluorescence imaging in vivo was taken at room temperature. Before measurements, *A. thaliana* was dark-adapted for 30 min at room temperature. The light parameters were as follows: measuring light intensity, 1; frequency, 1; actinic light intensity, 4; width, 0; saturation pulses intensity, 10; gain, 2; and damping, 1.

Flow cytometry

C. pyrenoidosa and *C. pyrenoidosa*/PBF were collected by centrifuging at 7000 rpm for 5 min. The precipitate was rinsed three times with deionized water and resuspended in BG-11 medium. The suspensions were analyzed by flow cytometer. The excitation laser was 488 nm. The detection channels were 610 and 680 nm for PBF and *C. pyrenoidosa*, respectively. For the cell cycle of *A. thaliana*, the leaves were cut from *A. thaliana* and placed in a petri dish. Nuclei Extraction Buffer (400 μl) was added. Then, the leaves were quickly chopped with a sharp blade. The cell suspensions were filtered into a sample tube for flow cytometry. Staining solution (800 μl; staining buffer,

propidium iodide, and ribonuclease A stock solution) was added into the tube. The sample was incubated for 15 min at room temperature in the dark and then was analyzed by flow cytometer.

SUPPLEMENTARY MATERIALS

Supplementary material for this article is available at http://advances.sciencemag.org/cgi/content/full/6/35/eabc5237/DC1

View/request a protocol for this paper from *Bio-protocol*.

REFERENCES AND NOTES

1. D. I. Arnon, Conversion of light into chemical energy in photosynthesis. *Nature* **184**, 10–21 (1959).
2. M. A. Borowitzka, High-value products from microalgae-their development and commercialisation. *J. Appl. Phycol.* **25**, 743–756 (2013).
3. J. G. Canadell, E. D. Schulze, Global potential of biospheric carbon management for climate mitigation. *Nat. Commun.* **5**, 5282 (2014).
4. P. G. Stephenson, C. M. Moore, M. J. Terry, M. V. Zubkov, T. S. Bibby, Improving photosynthesis for algal biofuels: Toward a green revolution. *Trends Biotechnol.* **29**, 615–623 (2011).
5. M. D. Ooms, C. T. Dinh, E. H. Sargent, D. Sinton, Photon management for augmented photosynthesis. *Nat. Commun.* **7**, 12699 (2016).
6. S. P. Long, E. A. Ainsworth, A. D. B. Leakey, P. B. Morgan, Global food insecurity. Treatment of major food crops with elevated carbon dioxide or ozone under large-scale fully open-air conditions suggests recent models may have overestimated future yields. *Philos. Trans. R. Soc. B Biol. Sci.* **360**, 2011–2020 (2005).
7. M. Chen, M. Schliep, R. D. Willows, Z. L. Cai, B. A. Neilan, H. Scheer, A red-shifted chlorophyll. *Science* **329**, 1318–1319 (2010).
8. M. Hambourger, G. F. Moore, D. M. Kramer, D. Gust, A. L. Moore, T. A. Moore, Biology and technology for photochemical fuel production. *Chem. Soc. Rev.* **38**, 25–35 (2009).
9. R. E. Blankenship, D. M. Tiede, J. Barber, G. W. Brudvig, G. Fleming, M. Ghirardi, M. R. Gunner, W. Junge, D. M. Kramer, A. Melis, T. A. Moore, C. C. Moser, D. G. Nocera, A. J. Nozik, D. R. Ort, W. W. Parson, R. C. Prince, R. T. Sayre, Comparing photosynthetic and photovoltaic efficiencies and recognizing the potential for improvement. *Science* **332**, 805–809 (2011).
10. L. Wondraczek, E. Tyystjarvi, J. Mendez-Ramos, F. A. Muller, Q. Zhang, Shifting the sun: solar spectral conversion and extrinsic sensitization in natural and artificial photosynthesis. *Adv. Sci.* **2**, 1500218 (2015).
11. L. Wondraczek, M. Batentschuk, M. A. Schmidt, R. Borchardt, S. Scheiner, B. Seemann, P. Schweizer, C. J. Brabec, Solar spectral conversion for improving the photosynthetic activity in algae reactors. *Nat. Commun.* **4**, 2047 (2013).
12. J. P. Giraldo, M. P. Landry, S. M. Faltermeier, T. P. McNicholas, N. M. Iverson, A. A. Boghossian, N. F. Reuel, A. J. Hilmer, F. Sen, J. A. Brew, M. S. Strano, Plant nanobionics approach to augment photosynthesis and biochemical sensing. *Nat. Mater.* **13**, 400–408 (2014).
13. C. E. Salesse-Smith, R. E. Sharwood, F. A. Busch, J. Kromdijk, V. Bardal, D. B. Stern, Overexpression of Rubisco subunits with RAF1 increases Rubisco content in maize. *Nat. Plants* **4**, 802–810 (2018).
14. S. Bellafiore, F. Barneche, G. Peltier, J. D. Rochaix, State transitions and light adaptation require chloroplast thylakoid protein kinase STN7. *Nature* **433**, 892–895 (2005).
15. W. J. Nawrocki, S. Stefano, L. Mosebach, F. -A. Wollman, F. Rappaport, State transitions redistribute rather than dissipate energy between the two photosystems in Chlamydomonas. *Nat. Plants* **2**, 16031 (2016).
16. G. Yang, L. Liu, Q. Yang, F. Lv, S. Wang, A multifunctional cationic pentathiophene: Synthesis, organelle-selective imaging, and anticancer activity. *Adv. Funct. Mater.* **22**, 736–743 (2012).
17. X. Feng, L. Liu, S. Wang, D. Zhu, Water-soluble fluorescent conjugated polymers and their interactions with biomacromolecules for sensitive biosensors. *Chem. Soc. Rev.* **39**, 2411–2419 (2010).
18. Y. Tang, F. Feng, M. Yu, L. An, F. He, S. Wang, Y. Li, D. Zhu, G. C. Bazan, Direct visualization of glucose phosphorylation with a cationic polythiophene. *Adv. Mater.* **20**, 703–705 (2008).
19. Y. Tang, F. Feng, F. He, S. Wang, Y. Li, D. Zhu, Direct visualization of enzymatic cleavage and oxidative damage by hydroxyl radicals of single-stranded DNA with a cationic polythiophene derivative. *J. Am. Chem. Soc.* **128**, 14972–14976 (2006).
20. S. W. Thomas, G. D. Joly, T. M. Swager, Chemical sensors based on amplifying fluorescent conjugated polymers. *Chem. Rev.* **107**, 1339–1386 (2007).
21. C. Zhu, L. Liu, Q. Yang, F. Lv, S. Wang, Water-soluble conjugated polymers for imaging, diagnosis, and therapy. *Chem. Rev.* **112**, 4687–4735 (2012).
22. L. Zhou, F. Lv, L. Liu, G. Shen, X. Yan, G. C. Bazan, S. Wang, Cross-linking of thiolated paclitaxel-oligo(*p*-phenylene vinylene) conjugates aggregates inside tumor cells leads to "chemical locks" that increase drug efficacy. *Adv. Mater.* **30**, 1704888 (2018).
23. Y. Wang, S. Li, L. Liu, F. Lv, S. Wang, Conjugated polymer nanoparticles to augment photosynthesis of chloroplasts. *Angew. Chem. Int. Ed.* **56**, 5308–5311 (2017).
24. X. Zhou, L. Zhou, P. Zhang, F. Lv, L. Liu, R. Qi, Y. Wang, M.-Y. Shen, H.-H. Yu, G. C. Bazan, S. Wang, Conducting polymers-thylakoid hybrid materials for water oxidation and photoelectric conversion. *Adv. Electron. Mater.* **5**, 1800789 (2018).
25. X. Zhou, P. Gai, P. Zhang, H. Sun, F. Lv, L. Liu, S. Wang, Conjugated polymer enhanced photoelectric response of self-circulating photosynthetic bioelectrochemical cell. *ACS Appl. Mater. Interfaces* **11**, 38993–39000 (2019).
26. G. Yang, L. Liu, F. Lv, S. Wang, Conjugated polyelectrolyte materials for promoting progenitor cell growth without serum. *Sci. Rep.* **3**, 1702 (2013).
27. R. Croce, H. van Amerongen, Natural strategies for photosynthetic light harvesting. *Nat. Chem. Biol.* **10**, 492–501 (2014).
28. L. O. Björn, *Photobiology: The Science of Light and Life Ch. 17*. (Springer, 2015).
29. E. Collini, C. Y. Wong, K. E. Wilk, P. M. Curmi, P. Brumer, G. D. Scholes, Coherently wired light-harvesting in photosynthetic marine algae at ambient temperature. *Nature* **463**, 644–647 (2010).
30. C. Safi, B. Zebib, O. Merah, P.-Y. Pontalier, C. Vaca-Garcia, Morphology, composition, production, processing and applications of *Chlorella vulgaris*: A review. *Renew. Sust. Energ. Rev.* **35**, 265–278 (2014).
31. D. H. Northcote, K. J. Goulding, R. W. Horne, Chemical composition and structure of the cell wall of *chlorella pyrenoidosa*. *Biochem. J.* **70**, 391–397 (1958).
32. H. Yuan, Z. Liu, L. Liu, F. Lv, Y. Wang, S. Wang, Cationic conjugated polymers for discrimination of microbial pathogens. *Adv. Mater.* **26**, 4333–4338 (2014).
33. H. M. Kalaji, G. Schansker, R. J. Ladle, V. Goltsev, K. Bosa, S. I. Allakhverdiev, M. Brestic, F. Bussotti, A. Calatayud, P. Dąbrowski, N. I. Elsheery, L. Ferroni, L. Guidi, S. W. Hogewoning, A. Jajoo, A. N. Misra, S. G. Nebauer, S. Pancaldi, C. Penella, D. B. Poli, M. Pollastrini, Z. B. Romanowska-Duda, B. Rutkowska, J. Serôdio, K. Suresh, W. Szulc, E. Tambussi, M. Yanniccari, M. Zivcak, Frequently asked questions about in vivo chlorophyll fluorescence: Practical issues. *Photosynth. Res.* **122**, 121–158 (2014).
34. T. Li, H. Kirchhoff, M. Gargouri, J. Feng, A. B. Cousins, P. T. Pienkos, D. R. Gang, S. Chen, Assessment of photosynthesis regulation in mixotrophically cultured microalga *Chlorella sorokiniana*. *Algal Res.* **19**, 30–38 (2016).
35. J. F. Allen, State transitions-a question of balance. *Science* **299**, 1530–1532 (2003).
36. Y. Ueno, S. Aikawa, A. Kondo, S. Akimoto, Adaptation of light-harvesting functions of unicellular green algae to different light qualities. *Photosynth. Res.* **139**, 145–154 (2019).
37. L.-S. Zhao, K. Li, Q.-M. Wang, X.-Y. Song, H.-N. Su, B.-B. Xie, X.-Y. Zhang, F. Huang, X.-L. Chen, B.-C. Zhou, Y.-Z. Zhang, Nitrogen starvation impacts the photosynthetic performance of *porphyridium cruentum* as revealed by chlorophyll a fluorescence. *Sci. Rep.* **7**, 8542 (2017).
38. Y.-T. Li, Y. Liang, Y.-N. Li, X.-K. Che, S.-J. Zhao, Z.-S. Zhang, H.-Y. Gao, Mechanisms by which Bisphenol A affect the photosynthetic apparatus in cucumber (*Cucumis sativus* L.) leaves. *Sci. Rep.* **8**, 4253 (2018).
39. C. Le Quiniou, B. van Oort, B. Drop, I. H. van Stokkum, R. Croce, The high efficiency of photosystem I in the green alga *Chlamydomonas reinhardtii* is maintained after the antenna size is substantially increased by the association of light-harvesting complexes II. *J. Biol. Chem.* **290**, 30587–30595 (2015).
40. B. M. Long, W. Y. Hee, R. E. Sharwood, B. D. Rae, S. Kaines, Y. L. Lim, N. D. Nguyen, B. Massey, S. Bala, S. von Caemmerer, M. R. Badger, G. Dean Price, Carboxysome encapsulation of the CO_2-fixing enzyme Rubisco in tobacco chloroplasts. *Nat. Commun.* **9**, 3570 (2018).
41. A. Krishan, Rapid flow cytofluorometric analysis of mammalian-cell cycle by propidium iodide staining. *J. Cell Biol.* **66**, 188–193 (1975).
42. H. Chong, C. Nie, C. Zhu, Q. Yang, L. Liu, F. Lv, S. Wang, Conjugated polymer nanoparticles for light-activated anticancer and antibacterial activity with imaging capability. *Langmuir* **28**, 2091–2098 (2012).

Acknowledgments: We thank K. Chong and Y. Xu of Institute of Botany, Chinese Academy of Sciences for guidance and assistance in *A. thaliana* culture and characterization. We also thank L. Liu for helping to take the SEM images and R. Qi for helping to measure ITC. **Funding:** This research was supported by the National Natural Science Foundation of China (nos. 21533012 and 21661132006) and Strategic Priority Research Program of the Chinese Academy of Sciences (no. XDA16020804). **Author contributions:** X.Z. and S.W. designed the research. X.Z., Y.Z., and Y.T. performed the experiments. X.Z., Y.H., F.L., and L.L. analyzed the data. X.Z. and S.W. wrote the paper. The manuscript was written through contributions of all authors. All authors have given approval to the final version of the manuscript. **Competing interests:** The authors declare that they have no competing interests. **Data and materials availability:** All data needed to evaluate the conclusions in the paper are present in the paper and/or the Supplementary Materials. Additional data related to this paper may be requested from the authors.

Submitted 29 April 2020
Accepted 13 July 2020
Published 26 August 2020
10.1126/sciadv.abc5237

Citation: X. Zhou, Y. Zeng, Y. Tang, Y. Huang, F. Lv, L. Liu, S. Wang, Artificial regulation of state transition for augmenting plant photosynthesis using synthetic light-harvesting polymer materials. *Sci. Adv.* **6**, eabc5237 (2020).